ELSEVIER

Journal of Structural Geology 28 (2006) 284–301

JOURNAL OF STRUCTURAL GEOLOGY

www.elsevier.com/locate/jsg

Fluid control of localized mineral domains in limestone pressure solution structures

Mark A. Evans [a,*], R. Douglas Elmore [b]

[a] *Department of Physics and Earth Science, Central Connecticut State University, New Britain, CT 06050, USA*
[b] *School of Geology and Geophysics, University of Oklahoma, Norman, OK 73019, USA*

Received 3 April 2005; received in revised form 4 October 2005; accepted 4 October 2005
Available online 2 December 2005

Abstract

Grain-to-grain and stylolitic solution structures in two central Appalachian Siluro–Devonian limestone macroscale folds contain one of four distinct mineral assemblages that are characterized by the dominant iron-phase mineral present: (1) chlorite ± illite ± *pyrite* ± calcite ± quartz ± TiO_2 ± goethite, (2) chlorite ± illite ± *pyrite altered to iron oxide/hydroxide* ± calcite ± quartz ± TiO_2, (3) chlorite ± illite ± *magnetite* ± calcite ± quartz, and (4) chlorite ± illite ± *goethite* ± calcite ± quartz ± TiO_2. Optical reflectance microscopy and SEM–EDS was used to characterize the mineralogy and mineral morphology of these structures. Geochemical modeling was used to constrain the conditions of formation and preservation.

The primary control on solution structure mineral assemblage was the redox conditions present in the solution structures during burial and deformation. The redox conditions on the microscale may have been controlled by the local fluid chemistry and the presence–absence of hydrocarbons and organic acids within the formation fluids, and the influx of externally derived fluids by fracture formation during the folding process. The wide variation in mineralogy of the solution structures shows that they were 'chemical factories' where a variety of chemical reactions took place during rock dissolution. In particular, the formation of authigenic magnetite in solution structures has significant implications for paleomagnetic applications, and use of anisotropy of anhysteretic remanent magnetization and anisotropy of magnetic susceptibility fabrics.

Keywords: Pressure solution; Stylolites; Magnetite; Fluid flow

1. Introduction

The stability of iron-minerals, such as pyrite, magnetite, hematite, and pyrrhotite, during burial diagenesis and deformation is of interest because of their importance in paleomagnetic studies (e.g. Leslie et al., 1990a,b; Johnson et al., 1995; Turner et al., 1995; Dinarés-Turell and Dekkers, 1999). Temperature, pressure, fluid chemistry, and subsurface redox conditions (Eh and pH) are the most important parameters controlling the chemistry of diagenetic reactions in sedimentary basins, and hence control the dissolution, alteration, and precipitation of these iron-minerals. However, environmental conditions are not static, but are constantly changing during sediment burial, diagenesis, and uplift (Burton et al., 1993; Machel, 1995; Turner et al., 1995). Hence, the mineralogy of the iron-phases also may change, resulting in (1) magnetization, (2) destruction of original magnetization, and/or (3) remagnetization of the rocks (e.g. Leslie et al., 1990b; Dinarés-Turell and Dekkers, 1999).

It is generally assumed that changes in environmental conditions can cause pervasive changes in iron-phase mineralogy throughout the rock, or minimally, near the walls of fractures or faults that demonstrably served as fluid conduits (e.g. Elmore et al., 1993a,b). However, several studies have shown that localized micromineral and microchemical domains exist in rocks due to fluid infiltration and diffusion processes along channelized pathways such as microcracks (Juster, 1987; McCaig and Knipe, 1990). Depending on the connectivity and communication with external fluid sources, these local fluid pathways could exhibit fluid chemistry and Eh–pH

* Corresponding author. Tel./fax: +1 860 832 2936.
E-mail address: evansmaa@ccsu.edu (M.A. Evans).

0191-8141/$ - see front matter © 2005 Elsevier Ltd. All rights reserved.
doi:10.1016/j.jsg.2005.10.004

conditions that could be significantly different than those within the host rock.

Pressure solution structures are of particular interest since they are pervasive in carbonate rocks, as well is in many clastic rocks (see Rutter (1983), Groshong (1988), and Passchier and Trouw (1996) for reviews of pressure solution phenomena). Significant amounts of host rock may be dissolved during pressure solution. For example, Tada and Siever (1989) in a review of previous work give a range of 5–34% volume loss in carbonate rocks while Davidson et al. (1998) and Markley and Wojtal (1995) suggest up to 50% volume loss may occur. The rock material lost during pressure solution must either precipitate locally in veins or be carried out of the local system by fluids. The expulsion of pressure-solved material may be accomplished by simple bed compaction and does not necessarily require a fluid flux of externally derived fluids. The 'insoluble' rock residue is then left behind in the form of a selvedge zone.

Solution structures act as discrete and preferential fluid conduits, thereby allowing the influx of external fluids and ions into the solution structures, as well as the removal of ions from the structures. Meike and Wenk (1988) have pointed to neocrystallized phyllosilicates and secondary calcite in solution structures as evidence that saturated fluids are moving through the seam during formation. Similarly, Bathurst (1971), Merino et al. (1983), Carozzi and von Bergen (1987), and Haubold (1999) suggest that stylolites may have porosity and permeability that would aid in localized, focused fluid flow. Enhanced porosity zones adjacent to stylolites have been documented by Carrio-Schffhauser et al. (1990) and Raynaud and Carrio-Schaffhauser (1992).

Although pressure solution zones are pervasive in most limestones, little work has been done to characterize the dissolution, alteration, and neocrystallization of minerals in the solution zones, and the chemical transitions and mass balance that occur within these zones. For example, Trurnit (1968) presented a sequence of minerals with decreasing relative pressure solubility. All minerals in the series that come after calcite can become part of the solution residue along a pressure solution surface in limestone. He concluded that hematite is equivalent to quartz in solubility, but no mention was made of magnetite, a common constituent in many limestones. Some authors have described the behavior of iron oxides as passive during pressure solution (Cox and Etheridge, 1989), whereby iron oxides are considered to be inert minerals tending to concentrate as residual phases along the foliation plane.

From a geochemical standpoint, Schwander et al. (1981) used microprobe and XRD/XRF to examine the difference between stylolite and host rock chemistry. He found that relatively insoluble clay minerals, quartz, K-feldspar, and pyrite were concentrated in stylolites while Ca and Mg were mobilized and partly removed from the system. Davidson et al. (1998) found that Ca and ^{18}O were depleted in cleavage ones while Mg, P, and Na were passively concentrated. Interestingly, they found that other elements, particularly K, Al, Si, Ti, and possibly Fe required significant metasomatic addition during deformation, resulting in neocrystallization of illite, kaolinite, quartz, and anatase. The end result is that the mineral assemblage within a pressure solution structure is significantly different from that of the host rock.

Detailed SEM–EDS (scanning electron microscope–electron dispersive spectra) analysis of stylolitic and grain-to-grain solution zones in Silurian and Devonian limestones from the central Appalachian Valley and Ridge province of West Virginia provide evidence for a variety of discrete mineral domains in pressure solution structures. The domains are characterized by mineral assemblages dominated by (1) iron oxide, (2) iron hydroxide, or (3) iron sulfide. In this paper we will characterize the mineralogy of three types of solution structures, and document the dissolution, alteration, and neocrystallization (?) of iron-phase minerals. In addition we will relate the mineral assemblages to the structural and fluid history of the rocks.

2. Geological setting

Limestones from the Upper Silurian Tonoloway Formation and the overlying Lower Devonian Helderberg Group were sampled from the macroscale Patterson Creek and the Wills Mountain anticlines in the Valley and Ridge province of northern West Virginia. The samples are from some of the same sample sites and retain the same sample numbers as those used by Evans et al. (2003) to characterize the anisotropy of magnetic susceptibility (AMS) and Lewchuk et al. (2003) to characterize the remanent magnetization.

Limestones of the Helderberg Group contain a wide range of lithologies including grainstones, wackestone, and carbonate mudstones (Dorobek and Read, 1986; Dorobek, 1987; Meyer and Dunne, 1990) but are dominated by coarse-grained lithologies. In contrast, the Tonoloway Formation is dominated by fine-grained lithologies such as carbonate mudstones and wackestones, although coarser grained rocks are occasionally present. Bedding parallel stylolites attributed to compaction are pervasive in both rock units. They account for up to 10–20%, and occasionally up to 35%, bed normal volume loss (Evans et al., 2003). In addition, solution structures that are normal to sub-normal to bedding are common. These are attributed to tectonic deformation and folding during the Alleghanian orogeny may account for up to 15% volume loss (Meyer and Dunne, 1990; Markley and Wojtal, 1995; Smart et al., 1997; Evans et al., 2003).

3. Methodology

3.1. Sampling

The samples were chosen to provide a wide variety of structural and stratigraphic positions within the folds. For

this study, only bed-parallel, compaction-related solution structures were investigated. The solution structures are discrete zones, ranging in thickness from <10 μm (grain-to-grain) to >500 μm (stylolitic) (Fig. 1), with each accounting for 10–1000 s of micrometer of volume loss normal to the structure. They have undulatory to serrated profiles, with amplitudes commonly up to 2 mm, and more rarely up to 10 mm.

3.2. Sample preparation and instrument description

Eleven limestone samples from the study of Evans et al. (2003) and one addition sample (73) were prepared for SEM observations by polishing thin sections in multiple steps to 0.3 μm alumina powder. The SEM used is a Philips XL-30 field emission scanning electron microscope equipped with detectors for imaging in secondary electron (SE) and backscattered electron (BSE) mode. Compositional analyses were done by energy-dispersive X-ray spectroscopy (EDS).

4. Solution structure mineral assemblages

4.1. Types of solution structures

In the Tonoloway and Helderberg limestones examined in this study, stylolite and grain to grain pressure solution zones fall into four general categories based on mineral assemblages that are characterized by the iron-phase minerals present.

4.1.1. Pyrite-bearing solution structures

These solution zones contain pyrite as the primary iron-phase mineral as determined by EDS analysis (Figs. 2 and 3a), with the general mineral assemblage (in order of decreasing abundance): chlorite $\pm$ illite $\pm$ *pyrite* $\pm$ calcite $\pm$ quartz $\pm$ TiO_2 (Table 1). The pyrite occurs as <1–20 μm anhedral to euhedral grains (Fig. 2b), and masses of submicron size grains, and less commonly as <20 μm framboids. The shapes and sizes of pyrite grains in the solution structures is the same as those grains found in the rock matrix, indicating passive concentration by solution.

4.1.2. Altered pyrite-bearing solution structures

Solution structures in the samples from sites 68 and 73 contain pyrite grains that are partially to completely altered for a general composition of chlorite $\pm$ illite $\pm$ *pyrite* $\rightarrow$ *iron oxide/hydroxide* $\pm$ calcite $\pm$ quartz $\pm$ TiO_2. Most contain a core of pyrite and a rim of iron oxide/hydroxide (Fig. 2d–f), which is interpreted to be goethite or magnetite based on EDS analysis (Fig. 3b and c) and the similarity in morphology to grains found by Xu et al. (1998) in limestones from Colorado. Other grains are completely altered to iron oxide/hydroxide (Fig. 2e and f). They commonly have a core and a ring of different brightness on backscatter electron micrographs. The rim and the core both give EDS spectra indicating a composition of iron and oxygen. Conventional EDS analysis does not produce accurate Fe/O rations, so it is not possible to distinguish between the common iron oxides (magnetite and hematite) and hydroxides (goethite) by EDS alone. In these two samples, common unaltered pyrite grains and uncommon altered pyrite grains are found in the rock matrix. However, all pyrite grains that are concentrated in the solution structures are partly to completely altered.

4.1.3. Magnetite-bearing solution structures

These solution zones contain an iron oxide mineral as the primary iron-phase mineral (Fig. 4a–f). These iron oxide grains are inferred to be magnetite based on (1) the sub-octahedral morphology of the grains, (2) EDS analysis that shows the presence of iron and oxygen along with minor silicon and calcium, which may be due to beam overlap on the surrounding material (Fig. 3d and e), and (3) rock magnetic work (Lewchuk et al., 2002, 2003) that shows magnetite to be the only remanence-carrying iron mineral in these rocks and that hematite is not present. The general

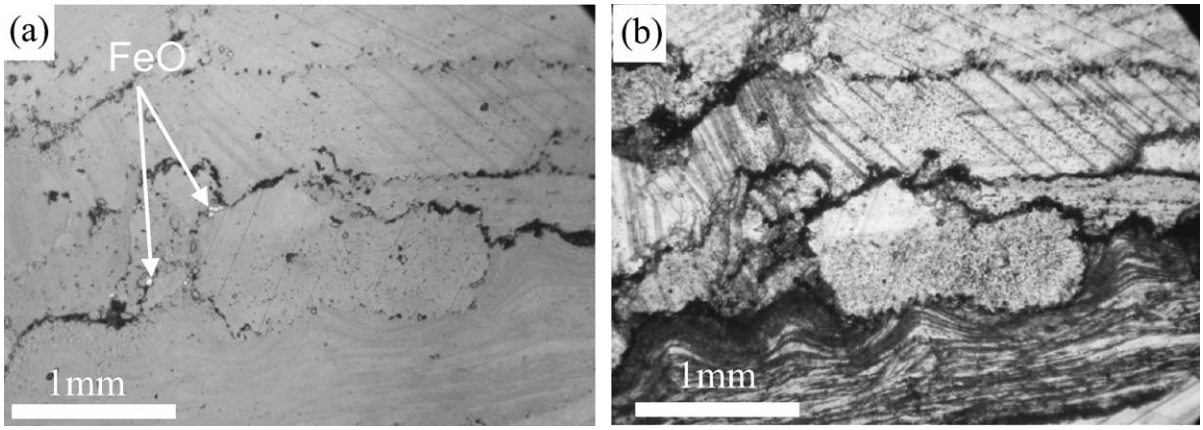

Fig. 1. (a) Reflectance and (b) optical PL photomicrographs of stylolitic solution structures between fossil fragments in samples of Helderberg grainstone. Note the selvedge zones consisting of 'insoluble' residue. Arrows in (a) point to micron-scale magnetite grains within the solution structures.

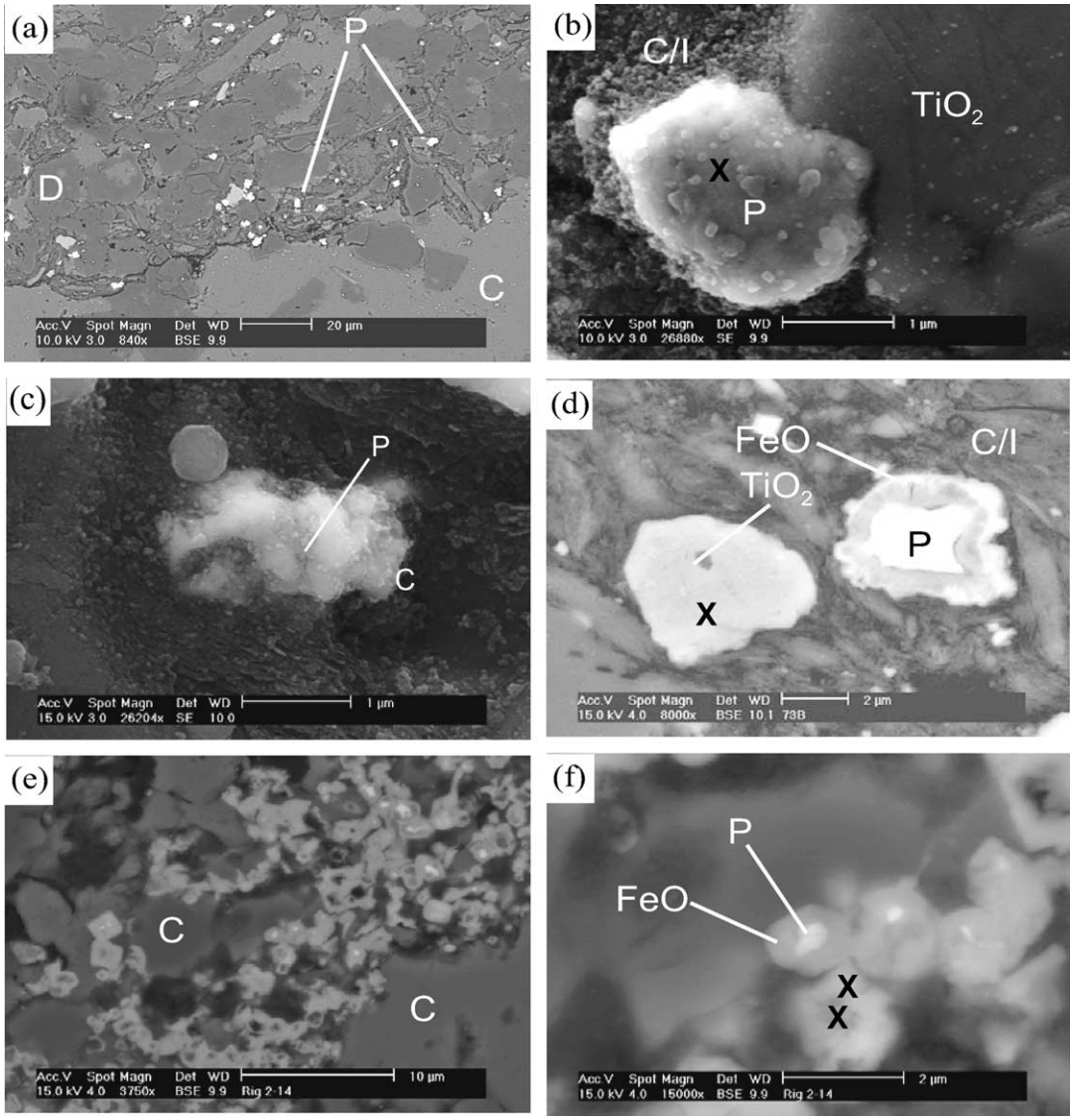

Fig. 2. Backscatter SEM images of (a) a pyrite-bearing solution structure, (b) pyrite grain pressure solving into a TiO_2 grain, (c) a mass of sub-micron pyrite, (d) pyrite with a rim of iron oxide adjacent to a TiO_2 grain, and (e) solution structure with pyrite partially to completely altered to iron oxide/hydroxide. The bright areas are pyrite, and the medium gray areas are an iron oxide/hydroxide (f) close-up of grain in (e) showing pyrite with an iron oxide rim and completely altered pyrite. C = calcite, C/I = chlorite/illite, FeO = iron oxide, P = pyrite, X = point of EDS spectra analysis shown in Fig. 3.

mineral assemblage of these solution structures is: chlorite ± illite ± *magnetite* ± calcite ± quartz (Table 1).

Magnetite occurs within the solution structures in one of three forms. First, uncommon framboids that are 3–20 µm in diameter (Fig. 4b and c) and composed of microcrysts that are <1 µm in diameter and have an octahedral to cubo-octahedral habit. Similar framboids have been described in other limestones (Lu et al., 1990; Suk et al., 1990a,b, 1991; Saffer and McCabe, 1992; Housen et al., 1993a), and have been interpreted as being magnetite altered from framboidal pyrite (Lu et al., 1990; Suk et al., 1990a; Housen et al., 1993a,b). Wilkins and Barnes (1997), on the other hand, argue that magnetite framboids are primary and form from the magnetic aggregation of individual microcrysts. Second, magnetite occurs as subcubic to irregular grains that are interpreted to be altered from pyrite or possibly siderite (Fig. 4c). In the samples that contain magnetite, pyrite is a common accessory in the host rock. However, pyrite is not found in these solution structures (Fig. 5), attesting to the markedly different environmental conditions within the stylolite structure as opposed to the host rock.

Finally, irregular aggregates (Fig. 4d–f) of individual crystals are commonly found within, and strung out along, the clay folia of the solution structures. These crystals are 0.05–1.0 µm in size, and fall into the range of single domain (SD) and pseudo-single domain (PSD) magnetic grains (Butler and Banerjee, 1975). The grains have an octahedral to sub-octahedral shape (within the limits of SEM resolution). The lower size limit is similar to that of biogenic magnetite, but the octahedral shape does not

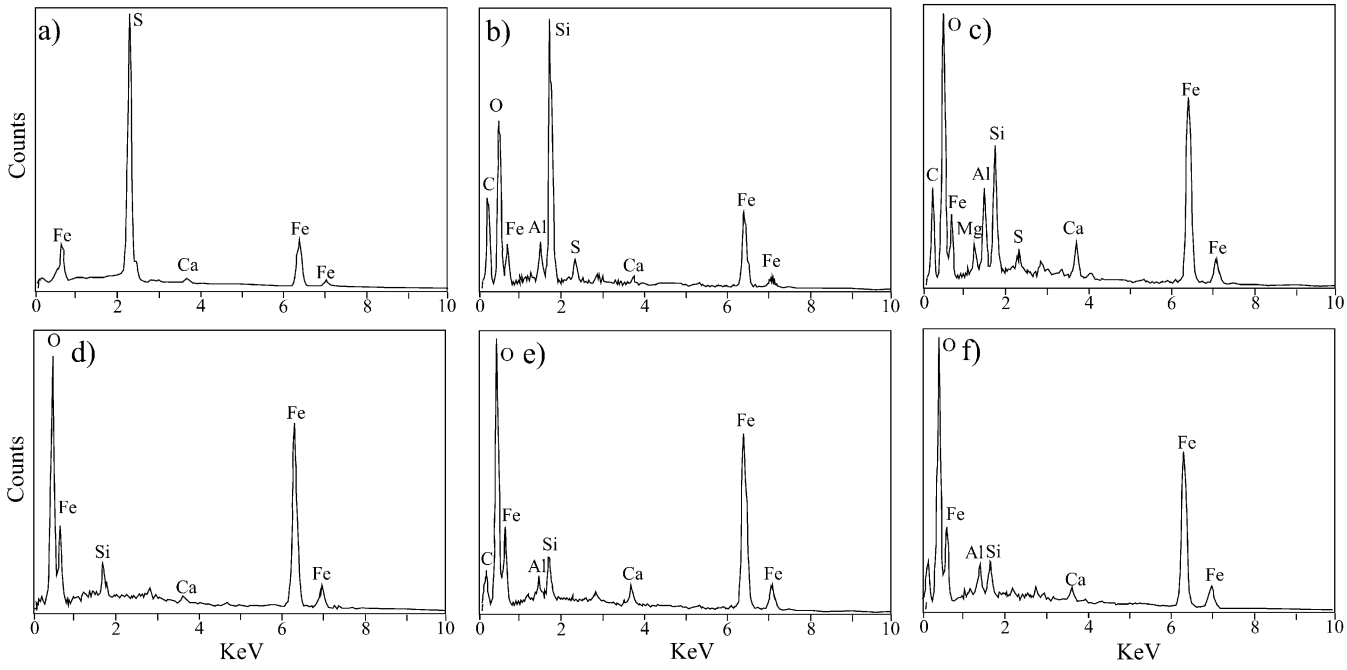

Fig. 3. Energy-dispersive spectra (EDS) of iron phase minerals in solution structures. (a) Pyrite grain in Fig. 2b, (b) rim (Fig. 2f, point *x*), and (c) core (Fig. 2f, point *y*) of pyrite grain altered to iron oxide/hydroxide. Note that some sulfur remains from the preexisting pyrite. (d) Sub-micron magnetite in Fig. 4f, (e) framboidal magnetite in Fig. 4c, and (f) goethite in Fig. 7c. Peaks due to C, O, Si, Mg, and Al are caused by beam overlap onto adjacent phases.

resemble the shapes of magnetite created by magnetotactic bacteria (Chang et al., 1987, 1989; Chang and Kirschvink, 1989; McNeill, 1990; Stoltz et al., 1990; Devourad et al., 1998). The crystals are always surrounded by aligned clays (Fig. 4d–f), and the clusters may occasionally be embayed into quartz grains (Fig. 4d). Their euhedral shape suggests that they are authigenic, and formed within the solution structures. Although not conclusive, detailed SEM scans of the limestone matrix of several samples failed to reveal similar grains outside the solution structures. Housen et al. (1993a) documented similar clusters of crystals in cleavage zones in Ordovician shales in Pennsylvania. Interestingly, we did not find any evidence of botryoidal or spheroidal magnetite as recognized in other limestones (e.g. McCabe et al., 1983; Suk et al., 1990a,b).

In several samples, magnetite framboids and clusters of sub-micron magnetite exhibit grain-to-grain dissolution. They are embayed into more soluble quartz grains (Fig. 4c

Table 1
Solution structure mineralogy

Site	Formation	Lithology	Bedding	Compaction solution strain (%)	ODU	Solution structure mineral assemblage
13	Helderberg	Packstone	208/30	11.5	99.7	Chlorite ± illite ± *goethite* ± calcite ± quartz ± TiO_2
17	Helderberg	Wackestone	022/45	12.0	13.0	Chlorite ± illite ± *magnetite* ± calcite ± quartz
46	Helderberg	Packstone	035/40	21.8	3.9	Chlorite ± illite ± *magnetite* ± calcite ± quartz
53	Helderberg	Wackestone	017/16	20.0	0.1	Chlorite ± illite ± *magnetite* ± calcite ± dolomite ± quartz ± K-feldspar
68	Helderberg	Packstone	032/30	35.0	96.1	Chlorite ± illite ± *pyrite* + *iron oxide/hydroxide* ± calcite ± quartz ± TiO_2
73	Helderberg	Wackestone	035/41	3.0	ND	Chlorite ± illite ± *pyrite* + *iron oxide/hydroxide* ± calcite ± quartz ± TiO_2
14	Tonoloway	Packstone	201/34	10.3	99.0	Chlorite ± illite ± *goethite* ± calcite ± quartz ± TiO_2
35	Tonoloway	Mudstone	052/32	21.0	39.6	Chlorite ± illite ± *magnetite* ± calcite ± quartz
38	Tonoloway	Wackestone	204/40	3.0	75.8	Chlorite ± illite ± *pyrite* + *iron oxide/hydroxide* ± calcite ± quartz ± TiO_2
51	Tonoloway	Wackestone	232/18	11.2	79.4	Chlorite ± illite ± *pyrite* ± calcite ± dolomite ± quartz ± TiO_2
78	Tonoloway	Wackestone	037/45	13.3	ND	Chlorite ± illite ± *goethite* ± calcite ± quartz ± TiO_2
83	Tonoloway	Mudstone	030/30	5.6	64.0	Chlorite ± illite ± *goethite* ± calcite ± quartz ± TiO_2

ODU, optimal differential unfolding. Data from Lewchuk et al. (2003). ND, no data.

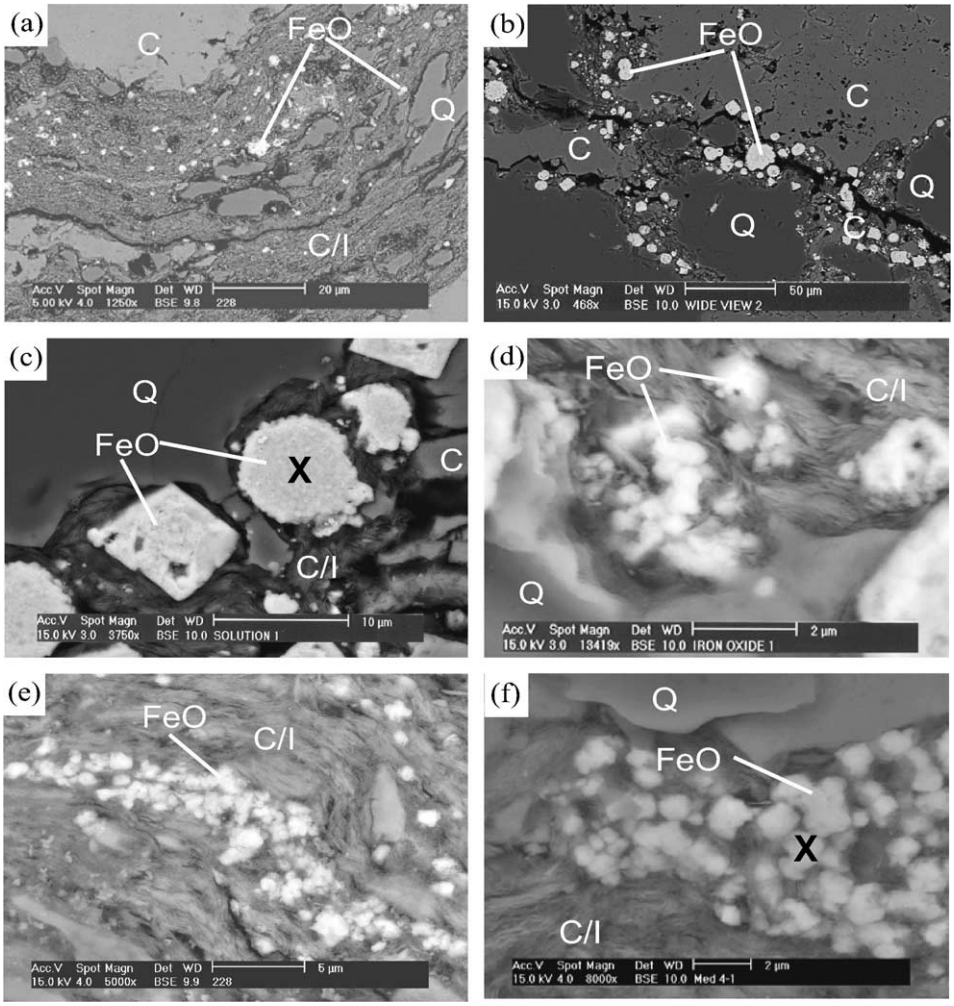

Fig. 4. (a) and (b) Backscatter SEM images of magnetite-bearing solution structures. Magnetite occurs as clusters of sub-micron size crystals, framboids interpreted to have been altered from pyrite, and large detrital or altered pyrite grains. (c) Close-up of (b) showing magnetite framboids and altered pyrite crystals with grain–grain dissolution and embayment into quartz. Note the presence of clays at the dissolution interface. (d) Euhedrl sub-micron magnetite grain embayed into quartz. (e) and (f) Close-ups of euhedral sub-micron magnetite grains in aligned chlorite/illite matrix. This magnetite is interpreted to have precipitated in the solution structure during deformation. C = calcite, C/I = chlorite/illite, M = magnetite, Q = quartz, X = point of EDS spectra analysis shown in Fig. 3.

and d), or exhibit mutual dissolution of framboids (Fig. 4b and c). At each dissolution boundary, there is a several micrometer thick clay film that may have assisted in the dissolution process by providing a water film diffusion pathway (Heald, 1956; Weyl, 1959; Wanless, 1979; Marshak and Engelder, 1985; Dewers and Ortoleva, 1990; Hickman and Evans, 1995). The strain induced dissolution of magnetite most likely occurs by phase-boundary

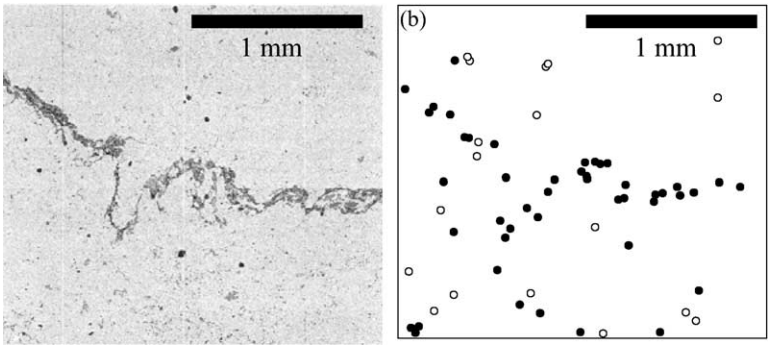

Fig. 5. (a) Backscatter SEM image of a solution structure. (b) SEM map of pyrite and iron oxide grains (> 1 mm) in the vicinity of the stylolite shown in a. Note the lack of pyrite in the solution structure and the corresponding increase in iron oxide. The iron oxide is interpreted to be magnetite in this sample.

hydrolysis of Fe^{2+}–O bonds at the magnetite surface and grain boundary diffusion of Fe^{2+}. At interphase boundaries of high normal stress, Fe^{2+}–O bonds are weakened (probably by substitution of Fe^{2+}–O bonds with weaker Fe^{2+}–OH bonds) and hydrolyzed (Lagoeiro, 1998).

As shown in Evans et al. (2003) anisotropy of anhysteretic remanent magnetization (AARM) ellipsoid anisotropies are high for these rocks, indicating a strong preferential orientation of magnetite grains. In particular, the short axes of the AARM ellipsoids are commonly bed normal, indicating a strong compaction component, and the long axes are aligned parallel to structural strike, indicating a tectonic influence. Inspection of the SEM images shows no discernable crystallographic alignment of iron oxide crystals at the given resolution. However, if the grains grew within the phyllosilicate folia, they may still contain a stress induced crystallographic orientation (Karato and Masuda, 1989). Housen and van der Pluijm (1991) and Housen et al. (1993a) found magnetite oriented parallel to cleavage in slates, concluding that the preferred orientation was most likely accomplished via dissolution and new growth of magnetite during cleavage formation.

4.1.4. Goethite-bearing solution structures

These solution zones contain goethite as the primary iron-phase mineral (Fig. 6a–f) as determined by EDS analysis (Fig. 3f), with the general mineral assemblage: chlorite ± illite ± *goethite* ± calcite ± quartz ± TiO_2 (Table 1). Goethite occurs as clusters and masses of radiating 0.5–1.0 μm long needles (Fig. 6e and f).

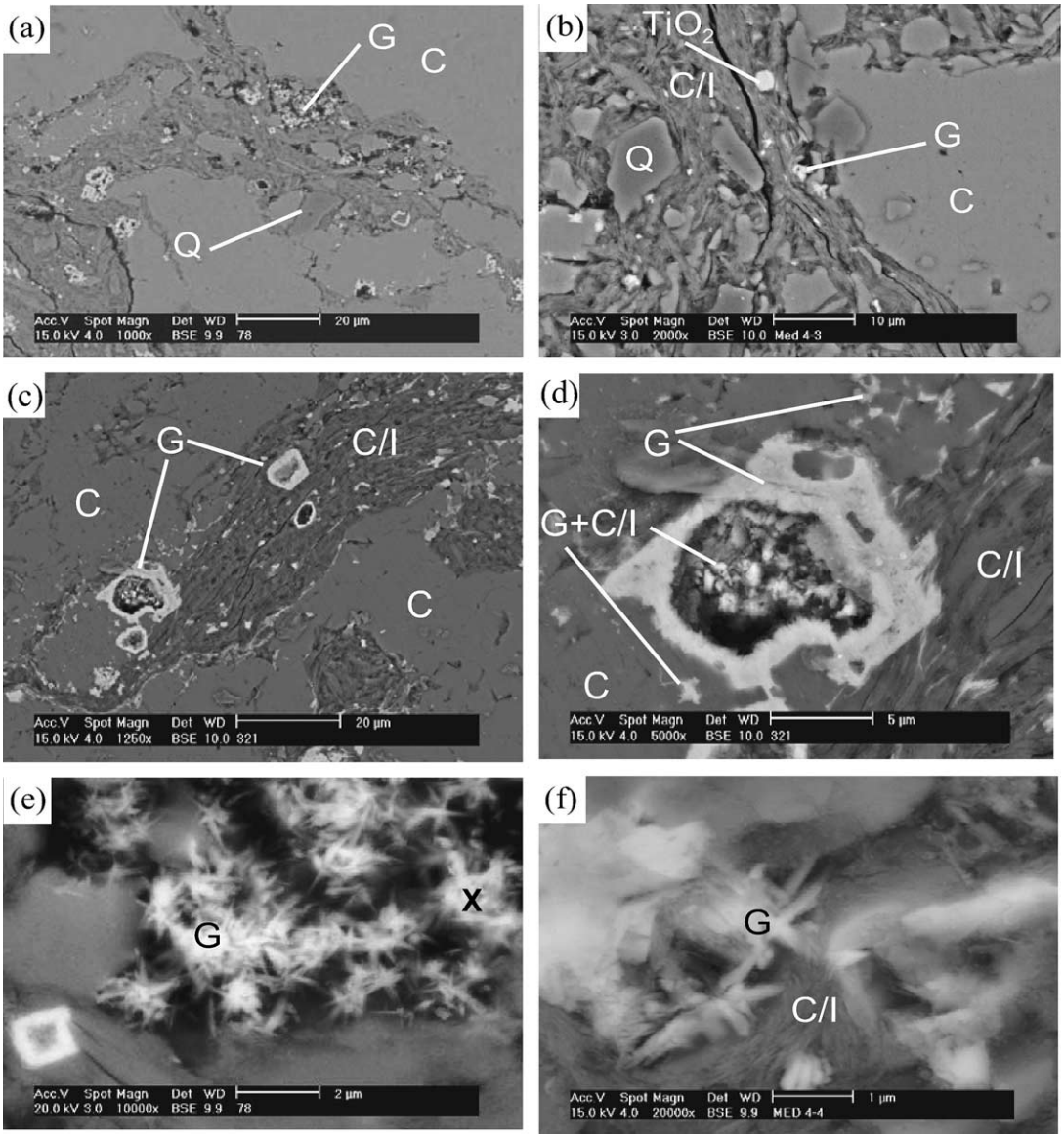

Fig. 6. (a)–(c) Backscatter SEM images of goethite-bearing solution structures. (d) Close-up of grains in (c). (e) and (f) Goethite showing distinctive needle-like habit. Peaks due to C, O, Si, Mg, and Al are caused by beam overlap onto adjacent phases. C = calcite, C/I = chlorite/illite, G = goethite, Q = quartz, X = point of EDS spectra analysis shown in Fig. 3.

Occasionally, goethite occurs as large (>5 μm) corroded subhedral grains (Fig. 6c and d) that may be altered magnetite or pyrite. Detailed SEM scans of the limestone matrix of several samples failed to reveal similar grains outside the solution structures.

4.2. Minerals common to most solution structures

4.2.1. Phyllosilicate minerals

The phyllosilicate minerals within the solution structures are interpreted to be a mixture of chlorite and illite based on the EDS analysis that indicate the presence of significant potassium, and magnesium, in addition to silicon, oxygen, and aluminum (Fig. 7a–c). Interestingly, phyllosilicates in goethite-bearing structures tend to be slightly more iron-rich than in other structures. The phyllosilicates show a strong preferred orientation parallel to the walls of the solution structures (Figs. 4a and e and 6b) and wrapping around less soluble grains such as quartz. Kreutzberger and Peacor (1988) have suggested that the accumulation and preferred orientation of the phyllosilicate minerals is due to passive accumulation by dissolution of the rock matrix and mechanical rotation within the solution structure. They also suggest that the phyllosilicates undergo little dissolution and crystallization during solution. On the other hand, Meike and Wenk (1988) have shown that phyllosilicate minerals precipitate and grow within the structures during deformation. Similarly, Holeywell and Tullis (1975) suggested that the preferred orientation of phyllosilicates in slaty cleavage was the result of preferred recrystallization under a nonhydrostatic stress rather than simply mechanical rotation of pre-existing minerals.

4.2.2. Authigenic quartz

Authigenic quartz is commonly found in the matrix of most fine-grained limestones as euhedral to subhedral grains on the order of 10–100 μm in the longest dimension. These grains are concentrated within the stylolite zone due to the lower solubility of quartz as compared with calcite. Within the stylolite, the quartz grains are highly corroded and embayed by less soluble mineral grains such as iron oxide, pyrite, and titanium oxide. Between each of the less soluble phases and the quartz there is usually a 1–3 μm layer of phyllosilicates (Fig. 4b and d). The quartz grains show a preferred shape orientation parallel to the stylolite boundaries (Fig. 4a), which may be due to either rigid-body rotation, and/or dissolution and reprecipitation in a stress field (Karato and Masuda, 1989). In either case, this provides evidence that the solution structures formed after the formation of authigenic quartz.

4.2.3. Titanium oxide

Irregular to subhedral, less than 4 μm diameter grains of titanium oxide (Figs. 2b and d and 6b), presumably anatase (TiO_2), are very common in pyrite-bearing and goethite bearing solution structures, but noticeably absent in magnetite-bearing solution structures. Similarly, these grains are generally absent in the host rock matrix. EDS spectra (Fig. 7d) show these grains to contain only titanium and oxygen. The mobility of titanium in solution structures has been a source of controversy. For example, Wintsch

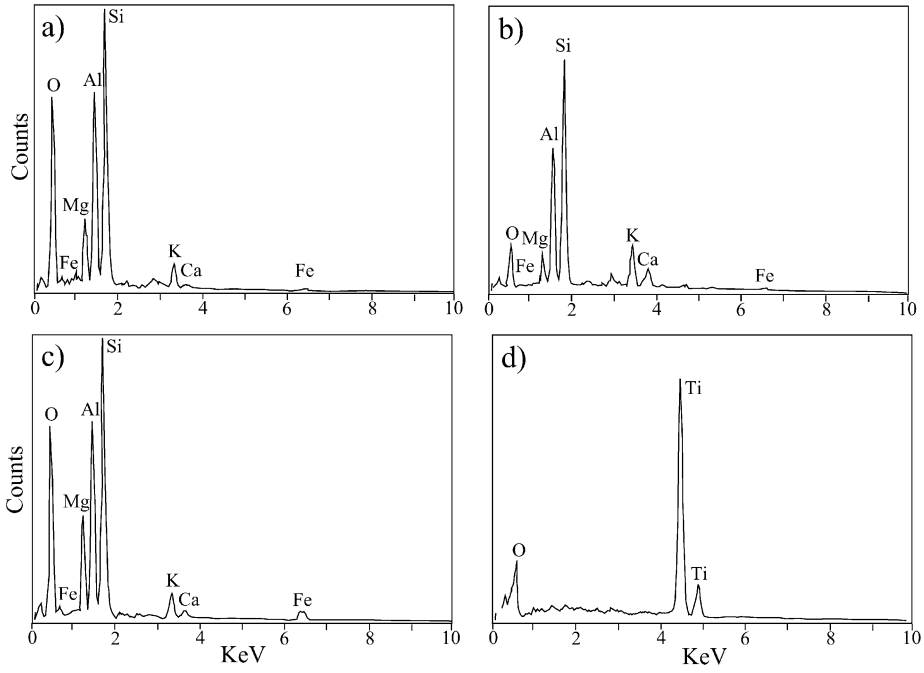

Fig. 7. (a)–(c) EDS spectra of clays in the three types of solution structures. All have a similar composition interpreted to be a combination of chlorite and illite. Clays in goethite bearing structures tend to be slightly more iron-rich. (d) EDS spectra of titanium oxide grain in Fig. 2d.

et al. (1991) in a study of cleavage zones in mudrocks found that titanium is relative immobile at the scale of solution zones and Schwander et al. (1981) suggest that titanium in limestone stylolites is immobile. On the other hand, Mimran (1977) and Davidson et al. (1998) show titanium to be very mobile and even requires metasomatic addition during deformation to reach observed concentrations in limestone solution structures. Similarly, Morad and Aldahan (1982, 1986)) found that titanium could be mobilized by dissolution of biotite and Fe–Ti oxides, such as illmenite, under reducing conditions at the microenvironment scale, with reprecipitation of titanium oxide. Such dissolution may take place in solution structures. Parnell (2004) makes a compelling case for titanium mobilization and precipitation by hydrocarbons. The passage of hydrocarbons through the Tonoloway and Helderberg Formations is documented by the presence of light liquid hydrocarbon fluid inclusions and bitumen inclusions in very early vein minerals.

4.2.4. Accessory minerals

Rarely, small (<3 μm) detrital apatite or zircon grains may be found in the solution structures, as well as occasional authigenic(?) K-feldspar, calcite, and dolomite. In addition, unusual phases such as a titanium–sulfur mineral, a copper–zinc mineral, a nickel mineral and even micron-size gold grains have been identified by EDS.

5. Environmental conditions during burial and deformation

5.1. Burial history diagram

In order to understand the environmental conditions present during burial and deformation, a burial history diagram (Fig. 8) was constructed for the Tonoloway and Helderberg Formations from the time of deposition through the Late Paleozoic Alleghanian orogeny. The diagram is constrained by published stratigraphic thicknesses (Reger and Tucker, 1924; Tilton et al., 1927) and restored stratigraphy based on paleo-overburdens and paleo-temperatures determined using fluid inclusion microthermometry (Fig. 9) (Evans and Battles, 1999; Evans and Hobbs, 2003). The onset of hydrocarbon generation in the Tonoloway–Helderberg section was determined by the compaction-corrected Lopatin method (Waples, 1980; Dykstra, 1987). Compaction during burial was accounted for using the method outlined in Baldwin and Butler, 1985). A geothermal gradient of 20 °C km^{-1} is used, with a surface

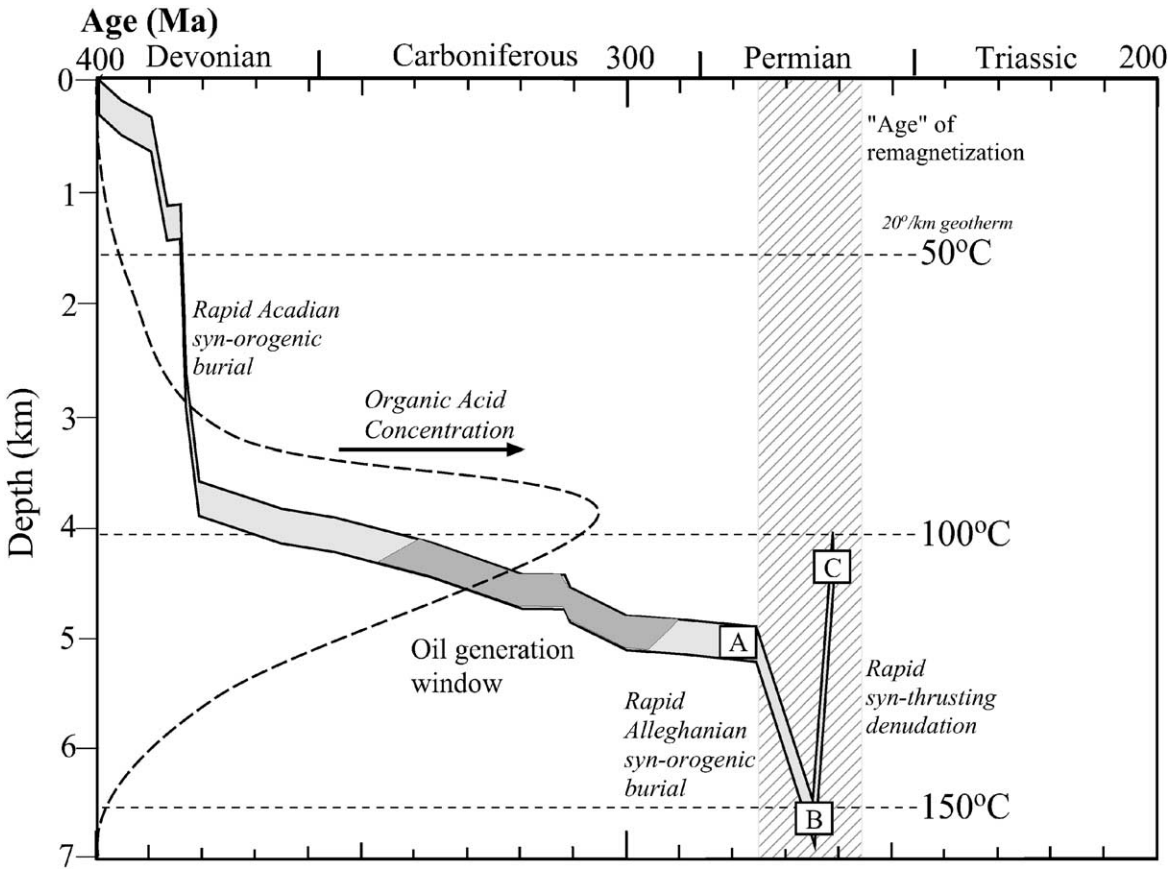

Fig. 8. Burial history curve for the Tonoloway and Helderberg Formations. Relative concentration of organic solvents curve modified from Surdam et al. (1989). Age of remagnetization from Stamatakos et al. (1996). Points A, B, and C are modeled conditions discussed in text.

temperature of 20 °C. Where possible, the type and composition of fluids present in the rocks during burial and deformation is determined from fluid inclusion microthermometry of pre- to syn-Alleghanian orogeny tectonic quartz and calcite veins (Evans and Battles, 1999).

5.2. Burial, deformation, and fluid history

After deposition, the Helderberg and Tonoloway limestones experienced rapid burial to a depth of approximately 3.5 km during the Late Devonian Acadian orogeny. In the 100 my between the Late Devonian and the Early Permian, there was an additional 1.5 km of burial, and organic material thermally matured to the point of generating liquid hydrocarbons (Figs. 8 and 10a). Peak liquid hydrocarbon generation occurred in the late Carboniferous and ceased by the beginning of the Permian as burial temperatures reached 120 °C and burial depths were approximately 5.0 km (point A on Fig. 8). The presence of hydrocarbons in the Tonoloway and Helderberg limestone rocks prior to and early during Alleghanian deformation is indicated by CH_4 and higher hydrocarbons (more than two carbon atoms) in vein mineral fluid inclusions and occasional bitumen fragments in vein material. Based on fluid inclusion microthemometry (Evans and Battles, 1999), the fluid present in the rocks during the Late Carboniferous to Early Permian was an in situ fluid in isotopic equilibrium with the host rock. The composition of the fluid is that of a $NaCl–CaCl_2$ rich brine with 20.5–25.8 wt% NaCl equivalent salinity. The fluid was saturated with CH_4 and contained up to 8 mole% CO_2. Coeval brine and methane fluid inclusions show that pore-fluid pressure was at or near lithostatic at 130 MPa (Evans and Battles, 1999). These fluid characteristics are comparable with fluids found in modern hydrocarbon-rich sedimentary basins (Morton and Land, 1987; Moldovanyi and Walter, 1992; Hanor, 1994).

During the Early Permian, syn-tectonic sedimentation associated with the advancing Alleghanian deformation front rapidly buried the region under at least an additional 2–4 km of Permian sediments (Figs. 8 and 10b) (Evans and Battles, 1999). Early during folding of the central Valley and Ridge province, the Middle Devonian through Upper Devonian rocks stratigraphically above the Tonoloway and Helderberg interval experienced the flow of ‘warm’ (approximately 200 °C), low-salinity (8.0–15.0 wt% NaCl equivalent), $NaCl–CaCl_2$ CH_4-rich brines from a hinterland source (Evans and Battles, 1999). This early syn-folding fluid migration event occurred at or near maximum burial of the western Valley and Ridge province (point B on Fig. 8). Coeval brine and methane fluid inclusions show that pore-fluid pressure was near lithostatic at 169 MPa, corresponding to a burial depth of 6.5 km (Evans and Battles, 1999). Although stable isotope data shows that the Tonoloway and Helderberg Formations were not altered by external fluids, some of the ‘warm’ fluids apparently infiltrated into the Helderberg limestone along open fractures (Fig. 9) (Dorobek, 1989; Evans and Battles, 1999).

The rocks in the study area then experienced a period of rapid syn-folding uplift and denudation associated with the transport of the Wills Mountain and Patterson Creek anticlines across a ramp in the Cambro–Odovician carbonate section (Fig. 10c and d). Rocks initially buried up to 6.5 km depth were uplifted to approximately 4.5 km depth. Subsequent transport emplaced the carbonate duplex

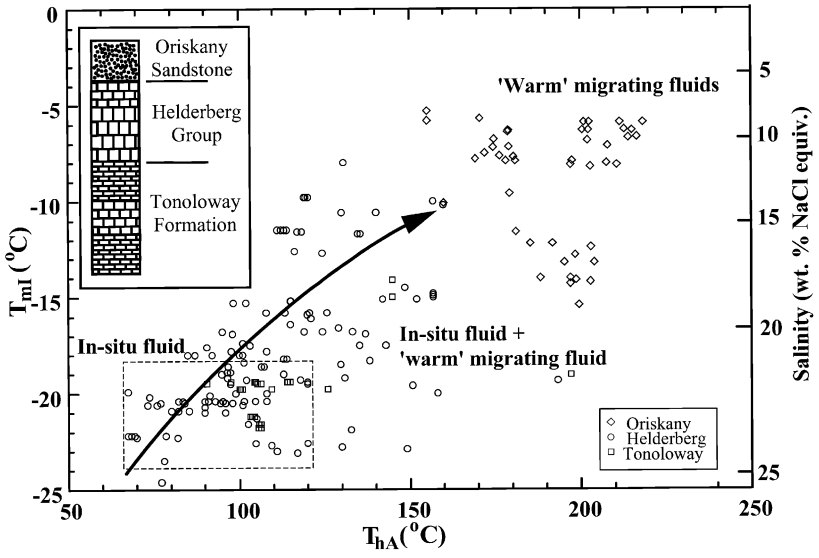

Fig. 9. Plot of Th versus Tm for fluid inclusions from calcite and quartz veins in the Tonoloway through Oriskany Formations in the Wills Mountain and Patterson Creek anticlines, West Virginia (data from Evans and Battles (1999), and unpublished data). The dashed box outlines unmodified formation fluid conditions. Note the mixing of Helderberg fluids with ‘warm’ low salinity fluids migrating trough the Oriskany sandstone. The Tonoloway, on the other hand, generally contains unmodified fluids. Arrow shows the interpreted mixing of ‘warm’ fluids with in situ formation fluids in the Helderberg limestones.

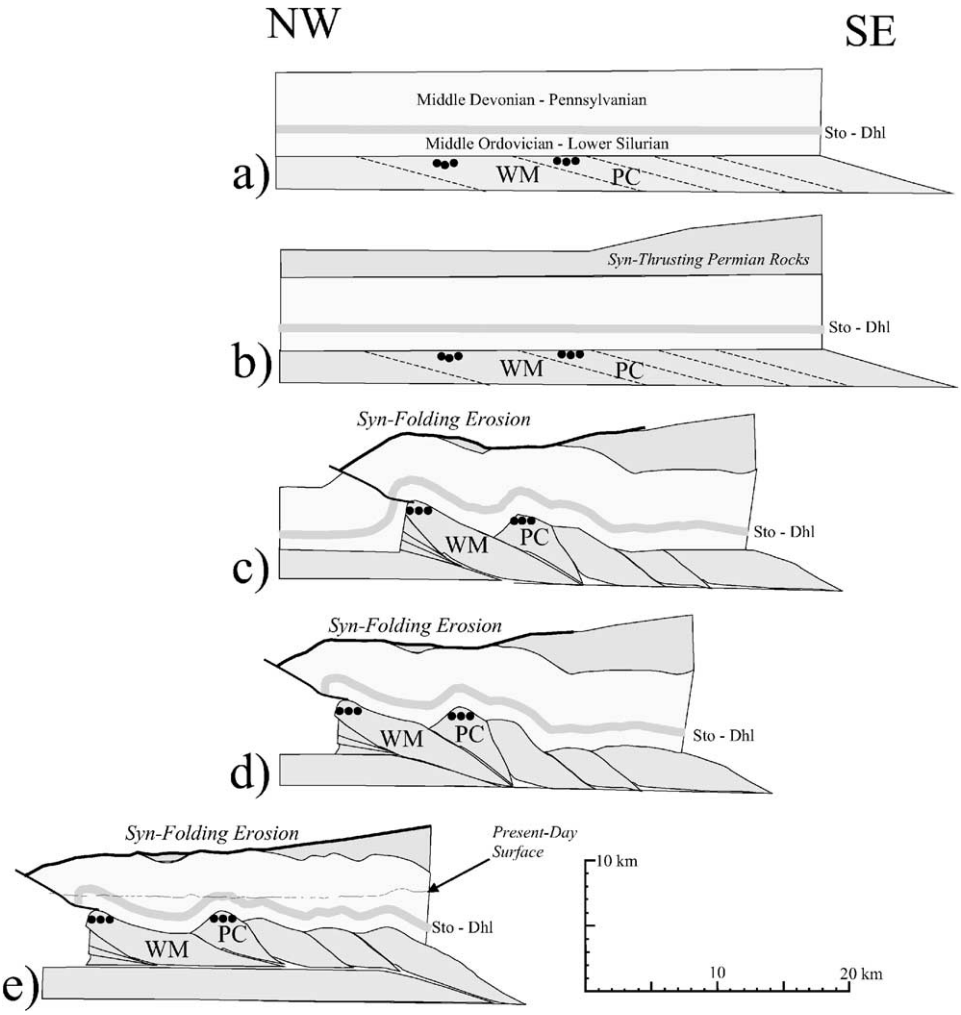

Fig. 10. Sequence of burial and deformation for the Wills Mountain anticline (WM) and Patterson Creek anticline (PC) in northern West Virginia. Based on burial and fluid history derived by Evans and Battles (1999), Evans and Hobbs (2003), and unpublished data. Sections (a), (c), and (e) correspond to points A, B, and C, respectively, on the burial history plot in Fig. 8. Locations of samples used in this study are schematically shown by small filled circles.

over 17 km of flat décollement forming the Nittany anticlinorium (Fig. 10e) (Wilson and Shumaker, 1992; Smart et al., 1997; Evans and Battles, 1999).

Although we have no direct evidence of the type of fluids present in the rocks after this period of rapid uplift and denudation, we assume that meteoric fluids were able to percolate into the breached structures along newly opened and reopened fractures. This increased fracturing and communication with the surface would have resulted in a drop of pore fluid pressures to near hydrostatic conditions. Deep penetration ($>$2–4 km depth) of meteoric fluids is well documented in modern and ancient structural settings (e.g. Nesbitt and Muehlenbachs, 1995; Shterev and Zagorchev, 1996; Varsanyi et al., 1999; Barker et al., 2000).

6. Oxidation–reduction modeling

Along with temperature, pressure, and fluid chemistry, subsurface redox conditions (Eh and pH) are the most important parameters controlling the chemistry of diagenetic reactions in sedimentary basins. The three different mineral assemblages found in the solution structures cannot coexist stably based on Eh–pH stability fields (Burton et al., 1993; Machel, 1995). Pyrite requires a high $\mathbf{a}[SO_4^{2-}]$, low Eh, and low pH; magnetite requires a low $\mathbf{a}[SO_4^{2-}]$, low Eh, and high pH; while goethite requires a low $\mathbf{a}[SO_4^{2-}]$, high Eh, and high pH. Therefore, in order to find all three mineral assemblages coexisting metastably in the same rocks, they had to have formed at different times and under different geochemical conditions.

In order to examine the effect of redox conditions on the mineralogy of iron phase minerals found in the Helderberg and Tonoloway Formations, three separate Eh–pH diagrams were calculated for three separate periods in the fluid-deformation history of the western Valley and Ridge province. The modeling was done using Geochemist's Workbench® (Bethke, 1998) Release 5.0 based on the thermodynamic database for SUPRCT92 by Johnson et al. (1991). For simplicity, we only took into account inorganic

Table 2
Chemistry of modeled brines

Modeled brine	T (°C)	P (MPa)	pH	TDS (mg/L)	Cl^- (mg/L)	SO_4^{2-} (mg/L)	HCO_3^- (mg/L)	Na^+ (mg/L)	Ca^{2+} (mg/L)	Mg^{2+} (mg/L)	K^+ (mg/L)	Fe^{2+} (mg/L)
Oilfield	120	130	5.9–7.0	22,0000	134,000	100	250	52,800	24,200	2000	1000	50
'Warm' migrating	200	169	7.0–8.0	120,000	73,200	10	200	28,800	13,200	1000	500	15
Deep meteoric	110	45	7.0–8.5	500	55	95	200	125	20	3	2	0.2

species and, although probably present, organic acids were not included in the modeling. Since microbial processes take place at temperatures less than 90 °C (Rozanova et al., 2001; Machal, 2004) they were also not considered.

6.1. Modeled conditions

6.1.1. Syn- to post-hydrocarbon generation

We can use modern oilfield brines as an analogue to model the Fe–O–H–C Eh–pH diagram applicable to the period just before rapid burial in the Early Permian. In modern sedimentary basins, pore water pH is very difficult to measure because of changes that occur as a sample is brought to the surface (Kharaka et al., 1986). Instead, geochemical modeling provides a good estimate of subsurface conditions. For example, computed pH values for oil field waters range from 4.0–5.5 in Pleistocene sands in the Gulf of Mexico (Kharaka et al., 1986) to 5.8–6.5 in Jurassic carbonates of Arkansas (Moldovanyi and Walter, 1992). Eh values in sedimentary basins are highly reducing, with Eh commonly less than −0.2 V due to the effect of dissolved organic species in the petroleum waters (Kharaka et al., 1980; Surdam and Crossey, 1985; Shebl and Surdam, 1996). The presence of H_2S in many oilfields also attests to the low Eh, and also to the presence of a large amount of sulfur. Hering and Stumm (1991) report that dissolution of iron oxides is markedly enhanced by reducing agents such as organic reductants, inorganic reductants, reduced metals in combination with organic ligands, or combinations of organic reductants and ligands. Similarly, Drummond and Palmer (1986) showed that acetate complexing contributed to significant iron oxide dissolution. Organic reductants and ligands such as acetate complexes are common constituents of oil and gas field waters (see review by Helgeson et al. (1993)).

The modeled brine composition (Table 2) is representative of oilfield brine analyses (Morton and Land, 1987; Moldovanyi and Walter, 1992; Hanor, 1994; Weaver et al., 1995; Hyeong and Capuano, 2001; Losh et al., 2002), and the measured fluid inclusion brine salinity from the Tonoloway and Helderberg Formations. We use $\mathbf{a}[SO_4^{2-}] = 10^{-5}$, $\mathbf{a}[Fe^{2+}] = 10^{-5}$, and $\mathbf{a}[HCO_3^-] = 10^{-3}$. Fluid inclusion data (Evans and Battles, 1999) give a temperature of approximately 120 °C, and pressures are near lithostatic at 130 MPa (burial depth of 5.0 km). The effect of pressure variation on the Eh–pH diagram is minimal in this range, so even if pressure were lower, say near a hydrostatic 50 MPa, the configuration of the Eh–pH diagram would not change significantly. These fluids would have been present in the rocks as the Alleghanian orogeny started and initial vein formation began.

6.1.2. Regional 'warm' fluid migration

The period of rapid syn-tectonic burial lead to in situ temperatures rising to nearly 160 °C and infiltration of 'warm' migrating fluids of approximately 200 °C. At

temperatures greater than 120 °C, decarboxylation reactions break down organic acids, and release CO_2 and bicarbonate (Surdam and Crossey, 1985) (Fig. 8), such that above 150 °C organic acid concentrations will be less than 100 mg/L (Helgeson et al., 1993). In these high-temperature, lower salinity fluids that have migrated from the hinterland, we assume that the organic acid content is minimal and that the sulfate content in markedly reduced from that of the oilfield fluid. We have no modern analogue of this 'warm' migrating brine. Instead, the modeled brine composition (Table 2) is based solely on the measured fluid inclusion brine salinity from the overlying Oriskany Formation. We use $\mathbf{a}[SO_4^{2-}]=10^{-8}$, $\mathbf{a}[Fe^{2+}]=10^{-6}$, and $\mathbf{a}[HCO_3^-]=10^{-3}$. We also assume that pH is somewhat higher, in the range of pH = 7.0–8.0 based on lowered organic acid content and the relationship that pH increases with decreasing salinity noted by Hanor (1994). We assume that Eh = −0.5 to −0.3, and is similar to oilfield waters because of the depth of the units (approximately 6.5 km), the lack of evidence for meteoric input, and the maintenance of lithostatic pressures (approximately 169 MPa) during maximum burial.

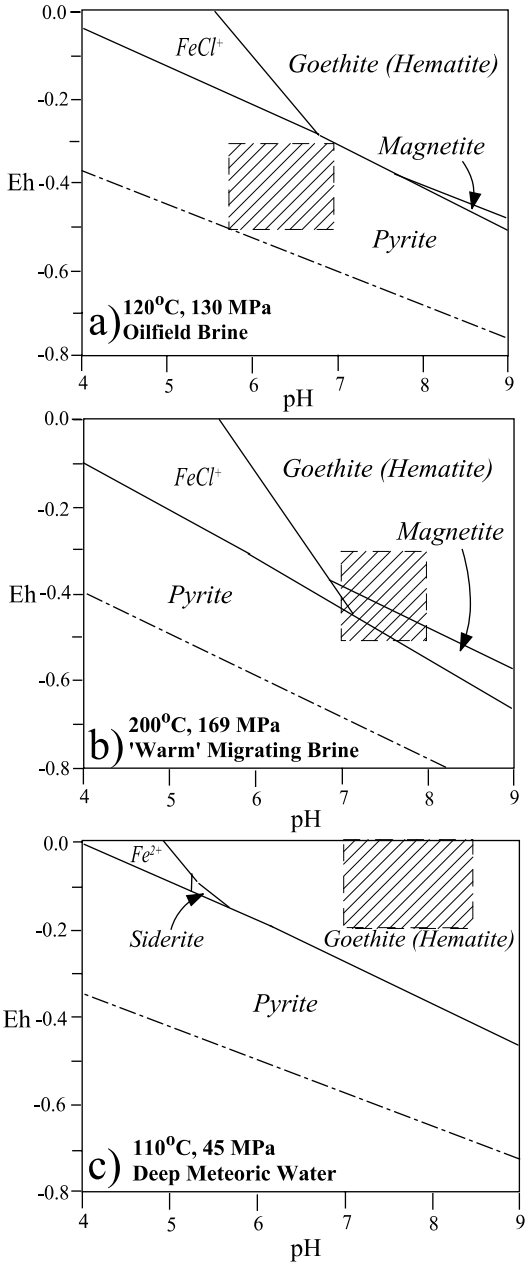

Fig. 11. Dependence of thermodynamic stabilities of iron minerals on Eh and pH in an aqueous environment. (a) Oil field waters with $\mathbf{a}[SO_4^{2-}]=10^{-5}$, $\mathbf{a}[Fe^{2+}]=10^{-5}$, and $\mathbf{a}[HCO_3^-]=10^{-3}$. (b) 'Warm' migrating brines with $\mathbf{a}[SO_4^{2-}]=10^{-8}$, $\mathbf{a}[Fe^{2+}]=10^{-6}$, and $\mathbf{a}[HCO_3^-]=10^{-3}$. (c) Deep meteoric waters with $\mathbf{a}[SO_4^{2-}]=10^{-3}$, $\mathbf{a}[Fe^{2+}]=10^{-6}$, $\mathbf{a}[HCO_3=10^{-3}$.

6.1.3. Syn-thrusting denudation and meteoric fluid influx

For the meteoric fluid influx, the modeled brine composition (Table 2) is representative of modern analogues from deep confined groundwaters in the Lincolnshire Limestone aquifer (Champ and Gulens, 1979), the chalk aquifer in the Berkshire syncline (Edmunds et al., 1987), the Tertiary aquifers near Mexico City (Edmunds et al., 2002), thermal fluids in peninsular India (Minissale et al., 2000), and the East Midlands Triassic sandstone aquifer (Smedley and Edmunds, 2002). These meteoric-derived fluids would have a higher Eh (−0.2 to +0.2 V) representing a more oxygen-rich system and somewhat higher pH (7.0–8.5) than basinal fluids. Therefore, we use $\mathbf{a}[SO_4^{2-}]=10^{-3}$, $\mathbf{a}[Fe^{2+}]=10^{-6}$, $\mathbf{a}[HCO_3^-]=10^{-3}$. For this interval, we use a temperature of 110 °C and a hydrostatic pressure of 45 MPa.

6.2. Modeling results

For the pressure–temperature conditions at position A in the burial history model, the pyrite stability field dominates the Eh–pH diagram (Fig. 11a), even at extremely reducing conditions. For more oxidizing conditions, at low pH values $FeCl^+$ is the stable phase, while hematite or iron hydroxide (goethite) would be stable at higher pH values. In general, goethite is the stable phase in the low-temperature and moderate- to high-pressure, hydrous environments modeled here (Posnjak and Merwin, 1922; Schmalz, 1959; Majzlan et al., 2003). For the inferred oil field waters present on the Tonoloway and Helderberg Formations at these conditions, pyrite is the stable phase. This is in agreement with Helgeson et al. (1993) who showed that most oil field waters in the Gulf coast are in equilibrium with siderite and/or pyrite.

For the pressure–temperature conditions at position B in the burial history model, the pyrite stability field dominates the Eh–pH diagram at reducing conditions (Fig. 11b). However, with increasing pH, magnetite becomes the stable phase. Again, at oxidizing conditions, iron hydroxide (goethite) would be stable, except at low pH values where aqueous $FeCl^+$ is the stable phase. For the inferred 'warm' migrating brines, fluid conditions lie on the magnetite field, with some overlap into both the pyrite and iron oxide/hydroxide fields. Any pre-existing pyrite would show

alteration to magnetite or iron hydroxide, and/or new magnetite and iron hydroxide may form.

After uplift and denudation, both pressure and temperature are lower than in earlier models. This results in the expansion of the pyrite stability field at the expense of the magnetite (Fig. 11c). Again, at oxidizing conditions, iron in the form of iron hydroxide would be stable at high pH values, while at low pH values, siderite or aqueous Fe^{2+} is the stable phase. For the inferred deep meteoric waters, fluid conditions are completely within the iron hydroxide field. Any preexisting pyrite or magnetite would alter to goethite and/or new iron hydroxide may form.

7. Discussion

7.1. Epidiagenesis of solution structure minerals

Because of the extended burial history of the Tonoloway and Helderberg Formations, it is difficult to determine the timing of compaction pressure solution. However, several workers (Dunnington, 1967; Bathurst, 1971; Buxton and Sibley, 1981) have suggested that in limestones, compaction stylolites can form very early in the diagenetic process, occurring at burial depths of less than 100 m. Based on studies of modern sea-floor sediments (e.g. Karlin, 1990; Leslie et al., 1990a,b) any primary biogenic magnetite present in the Tonoloway and Helderberg limestones was dissolved or altered to pyrite soon after burial as the sediments reached anoxic reducing conditions. This is supported by the lack of a primary paleomagnetic signature in these rocks (Elmore et al., 2001; Lewchuk et al., 2002, 2003). Therefore, we assume that the earliest-formed stylolites concentrated pyrite that was solved out of the sediment/rock matrix. With continued burial throughout the late Paleozoic, these early-formed stylolites, along with new stylolites, developed (Fig. 12a). With continued burial and oil generation, pyrite would continue to be the stable iron phase in the Tonoloway and Helderberg rocks. Concentrated diagenetic or authigenic pyrite in solution structures would remain stable.

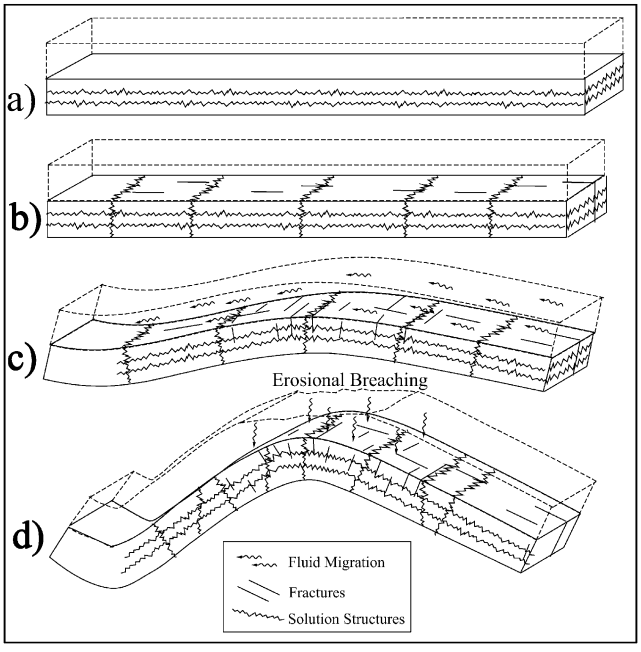

Fig. 12. Schematic sequence of burial and deformation showing evolution of fluid migration pathways in the Tonoloway and Helderberg Formations. (a) Initial burial with development of compaction solution structures. (b) Layer parallel shortening resulting in formation of extension fractures and tectonic stylolites. (c) Folding, accompanied by the formation of strike-parallel joints. These joints intersect some solution structures and allow the infiltration of 'warm' migrating fluids (arrows) from the overlying Oriskany Formation. (d) Post-folding erosional breaching of the fold allows infiltration of meteoric-derived waters (arrows) into the Tonoloway–Helderberg section.

As seen from the summary of stylolite mineralogy above, stylolites are 'chemical factories' where a variety of reactions take place during formation and enhancement. With the advent of Alleghanian deformation, two events controlled the changes in mineral chemistry of the solution structures. The changes are highly localized because, on the microscale, fluid chemistry may vary significantly depending on the stylolite connectivity and communication with external fluid sources.

First, folding of the Middle to Upper Devonian section resulted in the formation of planar, bed-normal, strike-parallel fractures and the opening of pre-folding Tectonic stylolites. The fractures preferentially formed in the competent thick-bedded Helderberg limestone layers, as opposed to the incompetent thin-bedded Tonoloway limestone. 'Warm' migrating fluids locally infiltrated along these fractures into the Helderberg, and possibly into the Tonoloway, from the Oriskany paleoaquifer above. Since the stylolite zones would have more permeability than the host rock matrix, the fluids would have then been able to infiltrate into stylolite zones that were in communication with the fractures. The infiltrating fluids would not have significantly altered the host rock as evidenced by oxygen and carbon stable isotope data (Evans and Battles, 1999) and strontium isotope data (Elmore et al., 2001). However, because of the inhomogeneity of the 'fracture plumbing' on the folds during the folding process, not all stylolites would see communication because they would not be in contact with a fracture. Therefore, only in preferentially oriented stylolites would pre-existing pyrite undergo alteration to magnetite, and authigenic magnetite be precipitated. The source of the iron for authigenic magnetite could be: (1) structural ordering of mixed-layer smectite to illite releasing Fe^{3+} (Boles and Franks, 1979; Surdam and Crossey, 1985; Lu et al., 1991; Katz et al., 1998, 2000); (2) dissolution of ferroan calcite (Dorobek, 1987) in the rock matrix; (3) alteration of pyrite within the host rock (Suk et al., 1990a; Brothers et al., 1996); (4) dissolution of detrital biotite or illmenite; or (5) hydrocarbons (Ellrich et al., 1985).

Second, during transport of the duplex and cover rocks across the Wills Mountain ramp, the cover rock sequence was fractured again, and synthrusting erosion of the rising anticlinorium breached the regional overpressure seal (Fig. 12b). This allowed the influx of oxygen-rich meteoric-derived water into the Tonoloway–Helderberg section, along optimally oriented opened fractures. These fractures again would have allowed these fluids to locally infiltrate stylolite zones in contact with the fracture. The breaching of the overpressure seal may have also enhanced the pressure solution process by increasing grain-to-grain stresses (Thomas et al., 1993). Again, this period of epidiageneis (Dinarés-Turell and Dekkers, 1999) would not have significantly modified the host rock isotope chemistry.

7.2. Implications for rock magnetic response

Solution structures such as stylolites and cleavage have been suggested as important contributors to alteration of rock remanent magnetism (Kodama, 1988; Housen and van der Pluijm, 1991; Lewchuk et al., 2002) and AMS response (Borradaile, 1988; Imaz et al., 2000; Evans et al., 2003). The two limestone formations examined in this study were remagnetized during the Permian Kiaman event (Evans et al., 2000; Lewchuk et al., 2003). The timing of this regional remagnetization has been placed between ca. 255 and 275 Ma (Stamatakos et al., 1996).

Analysis of Silurian and Devonian limestones in West Virginia has shown there is a direct link between the amount of rock dissolution strain with the apparent timing of rock remagnetization with respect to folding and the AMS fabric (Lewchuk et al., 2003). The relationship is one where rocks with little or no pressure solution strain contain a pre-folding remagnetization, but as solution strain increases, the remagnetization appears to be more syn-folding Lewchuk et al., 2002, 2003). Small circle statistical analysis (Shipunov, 1997) using the optimal differential untilting (ODU) technique of Enkin et al. (2000) was used to determine to what extent individual paleomagnetic site means within each fold shared a common direction during unfolding. The advantage of this test is that it untilts each site individually at differing rates to derive a common direction from the intersection of their small circle paths from geographic to stratigraphic coordinates, rather than untilting each limb symmetrically to the best grouping of site directions. The result yields a set of untilting percentages for each site at this shared direction. For these samples, ODU is strongly related to the type of iron phase mineral in the solution structures (Table 1). The ODU values are very low (<40, syn-folding remagnetization) for rock that have solution structures containing magnetite, while rocks that have solution structures with pyrite or goethite have ODU values greater than 40 (pre-folding remagnetization). This suggests that the infiltration of syn-deformational fluids into solution structures and the growth authigenic magnetite along with the alteration of pre-existing iron phases may exert important controls on the syn-folding character of the rocks. Clearly, this is an area that needs further testing.

8. Conclusions

Limestone solution structures from the Tonoloway and Helderberg Formations show three distinct mineral assemblages dominated by iron-phase minerals: pyrite, magnetite, and goethite. The primary control on solution structure mineral assemblage was the redox conditions present in the solution structures during burial and deformation. The redox conditions on the microscale may have been controlled by the local fluid chemistry and the presence–absence of hydrocarbons and organic acids within the formation fluids, and the influx of externally derived fluids by fracture formation during the folding process. The types of fluids in the solution structures varied significantly over time depending on the connectivity and communication with external fluid sources. Earliest fluids were hydrocarbon-rich, high-salinity brines that were generally reducing and favored pyrite stability. As folding commenced, ‘warm’ low-salinity brines locally infiltrated along fractures, causing the alteration of pyrite to iron oxide/hydroxide and the precipitation of authigenic magnetite. Finally, breaching of the folds by fracturing allowed communication with oxidizing meteoric fluids and formation of goethite in the solution structures. In general, the external fluids did not significantly affect the relatively impermeable limestone matrix, but were focused along the more permeable solution structures. The wide variation in mineralogy of the solution structures shows that they are ‘chemical factories’ where a variety of chemical reactions take place during rocks dissolution and fluid influx. In particular, the formation of authigenic magnetite in solution structures during burial and deformation has significant implications for paleomagnetic applications, and use of AARM and AMS fabrics.

Acknowledgements

We acknowledge the support for this project from National Science Foundation grant EAR-9814913 to Evans and Elmore. We also thank J. Blachere and A. Stewart for assisting in the SEM work, as well as S. Kennedy and R.J. Lee Instruments, Inc. for use of the Personal SEM.

References

Baldwin, B., Butler, C.O., 1985. Compaction curves. AAPG Bulletin 69, 622–625.

Barker, A.J., Bennett, D.G., Boyce, A.J., Fallick, A.E., 2000. Retrogression by deep infiltration of meteoric fluids into thrust zones during late-orogenic rapid unroofing. Journal of Metamorphic Geology 18, 307–318.

Bathurst, R.G.C., 1971. Carbonate Sediments and their Diagenesis. Elsevier, New York.

Bethke, C.M., 1998. The Geochemist's Workbench. University of Illinois, Illinois.

Boles, J.R., Franks, S.G., 1979. Reply cementation of sandstones. Journal of Sedimentary Petrology 49, 1362.

Borradaile, G.J., 1988. Magnetic susceptibility, petrofabrics and strain. Tectonophysics 10, 1–20.

Brothers, L.A., Engle, M.H., Elmore, R.D., 1996. The late diagenetic conversion of pyrite to magnetite by organically complexed ferric iron. Chemical Geology 130, 1–14.

Burton, E.A., Machel, H.G., Qi, J., 1993. Thermodynamic constraints on anomalous magnetization in shallow and deep hydrocarbon seepage environments. In: Aïssaoui, D.M., McNeill, D.F., Hurley, N.F. (Eds.), Applications of Paleomagnetism to Sedimentary Geology SEPM Special Publication 49, pp. 194–207.

Butler, R.F., Banerjee, S.K., 1975. Theoretical single-domain grain size range in magnetite and titanomagnetite. Journal of Geophysical Research 80, 4049–4058.

Buxton, T.M., Sibley, D.G., 1981. Pressure solution features in shallow buried limestone. Journal of Sedimentary Petrology 51, 19–26.

Carozzi, A.V., von Bergen, D., 1987. Stylolitic porosity in carbonates: a critical factor in deep hydrocarbon production. Journal of Petroleum Geology 10, 267–282.

Carrio-Schffhauser, E., Raynaud, S., Latiére, H.J., Mazerolle, F., 1990. Propagation and localization of stylolites in limestones. In: Knipe, R.J., Rutter, E.H. (Eds.), Deformation Mechanisms, Rheology and Tectonics Geological Society Special Publication 54, pp. 193–199.

Champ, D.R., Gulens, J., 1979. Oxidation-reduction sequences in groundwater flow systems. Canadian Journal of Earth Sciences 16, 12–23.

Chang, S-B.R., Kirschvink, J.L., 1989. Magnetofossils, the magnetization of sediments, and the evolution of magnetite biomineralization. Annual Reviews of Earth and Planetary Science 17, 169–195.

Chang, S-B.R., Kirschvink, J.L., Stoltz, J.F., 1987. Biogenic magnetite as a primary remanence carrier in limestone deposits. Physics of the Earth and Planetary Interiors 46, 289–303.

Chang, S-B.R., Stoltz, J.F., Kirschvink, J.L., Awramik, S.M., 1989. Biogenic magnetite in stromatolites. II. Occurrence in ancient sedimentary environments. Precambrian Research 43, 305–315.

Cox, S.F., Etheridge, M.A., 1989. Coupled grain-scale dilatancy and mass transfer during deformation at high fluid pressures: examples from Mount Lyell, Tasmania. Journal of Structural Geology 11, 147–162.

Davidson, S.G., Anastasio, D.J., Bebout, G.E., Holl, J.E., Hedlund, C.A., 1998. Volume loss and metasomatism during cleavage formation in carbonate rocks. Journal of Structural Geology 20, 705–726.

Devourad, B., Pósfal, M., Hua, X., Bazylinski, D.A., Frankel, R.B., Buseck, P.R., 1998. Magnetite from magnetotactic bacteria: size distribution and twinning. American Mineralogist 83, 1387–1398.

Dewers, T., Ortoleva, P., 1990. A coupled reaction/transport/mechanical model for intergranualr pressure solution and cementation in clean sandstones. Geochimica et Cosmochimica Acta 54, 1609–1625.

Dinarés-Turell, J., Dekkers, M.J., 1999. Diagenesis and remanence acquisition in the lower Pliocene Trubi marls at Punta di Maiata (southern Sicily); palaeomagnetic and rock magnetic observations. In: Tarling, D.H., Turner, P. (Eds.), Paleomagnetism and Diagenesis in Sediments Geological Society Special Publication 151, pp. 53–69.

Dorobek, S., 1987. Petrography, geochemistry, and origin of Burial diagenetic facies, Silurio-Devonian Helderberg Group (carbonate rocks), central Appalachians. American Association of Petroleum Geologists Bulletin 71, 492–514.

Dorobek, S., 1989. Migration of orogenic fluids through the Siluro-Devonian Helderberg Group during late plaoezoic deformation: constraints on fluid sources and implications for thermal histories of sedimentary basins. Tectonophysics 159, 25–45.

Dorobek, S., Read, J.F., 1986. Sedimentology and basin evolution of the Siluro-Devonian Helderberg Group, central Appalachians. Journal of Sedimentary Petrology 56, 601–613.

Drummond, S.E., Palmer, D.A., 1986. Thermal decarboxylation of acetate. Part 1. The kinetics and mechanism of reaction in aqueous solution. Geochimica et Cosmochimica Acta 50, 813–823.

Dunnington, H.V., 1967. Aspects of diagenesis and shape change in stylolitic limestone reservoirs. Seventh World Petroleum Congress Proceedings, Mexico 2, 339–352.

Dykstra, J., 1987. Compaction correction for burial history curves: application to Lopatin's method for source rock maturation determination. Geobyte 2, 16–23.

Edmunds, W.M., Cook, J.M., Darlling, W.G., Kinniburgh, D.G., Miles, D.L., Bath, A.H., Morgan-Jones, M., Andrews, J.N., 1987. Baseline geochemical conditions in the chalk aquifer, Berkshire, UK: a basis for groundwater quality management. Applied Geochemistry 2, 251–274.

Edmunds, W.M., Carrillo-Rivera, J.J., Cardona, A., 2002. Geochemical evolution of groundwater beneath Mexico City. Journal of Hydrology 258, 1–24.

Ellrich, J., Hirner, A., Stark, H., 1985. Distribution of trace elements in crude oils from southern Germany. Chemical Geology 48, 313–323.

Elmore, R.D., London, D., Bagley, D., Fruit, D., Gao, G., 1993a. Remagnetizatiton by basinal fluids: testing the hypothesis in the Viola limestone, southern Oklahoma. Journal of Geophysical Research 98, 6237–6254.

Elmore, R.D., London, D., Bagley, D., Gao, G., 1993b. Evidence of paleomagnetic dating of diagenesis by basinal fluids, Ordovician carbonates, Arbuckle mountains, southern Oklahoma. In: Aïssaoui, D.M., McNeill, D.F., Hurley, N.F. (Eds.), Applications of Paleomagnetism to Sedimentary Geology Society for Sedimentary Geology Special Publication 49, pp. 115–128.

Elmore, R.D., Kelly, J., Evans, M.A., Lewchuk, M.T., 2001. Remagnetization and orogenic fluids: testing the hypothesis in the central Appalachians. Geophysical Journal International 144, 568–576.

Enkin, R.J., Osadetz, K.G., Baker, J., Kisilevsky, D., 2000. Orogenic remagnetization in the front ranges and inner foothills of the Southern Canadian Cordillera: chemical harbinger and thermal handmaiden of Cordilleran deformation. Geological Society of America Bulletin 112, 929–942.

Evans, M.A., Battles, D.A., 1999. Fluid inclusion and stable isotope analysis of veins from the central Appalachian Valley and Ridge province: implications for regional synorogenic hydrologic structure and fluid migration. Geological Society of America Bulletin 111, 1841–1860.

Evans, M.A., Hobbs, G.C., 2003. Fate of 'warm' migrating fluids in the central Appalachians during the Late Paleozoic Alleghenian orogeny. Journal of Geochemical Exploration 78–79, 327–331.

Evans, M.A., Elmore, R.D., Lewchuk, M.T., 2000. Examining the relationship between remagnetization and orogenic fluids: central Appalachians. Journal of Geochemical Exploration 69–70, 139–142.

Evans, M.A., Lewchuk, M.T., Elmore, R.D., 2003. Strain partitioning and deformation mechanisms in limestones: examining the relationship of strain and anisotropy of magnetic susceptibility (AMS). Journal of Structural Geology 25, 1525–1549.

Groshong Jr., R.H., 1988. Low temperature deformation mechanisms and their interpretation. Geological Society of America Bulletin 100, 1329–1360.

Hanor, J.S., 1994. Origin of saline fluids in sedimentary basins. In: Parnell, J. (Ed.), Geofluids: Origin, Migration and Evolution of Fluids in Sedimentary Basins. Geological Society Special Publication 78, pp. 151–174.

Haubold, H., 1999. Alteration of magnetic properties of Paleozoic platform carbonate rocks burial diagnesis (Lower Ordovician sequence, Texas, USA). In: Tarling, D.H., Turner, P. (Eds.), Paleomagnetism and Diagenesis in Sediments. Geological Society, London, Special Publication 151, pp. 181–203.

Heald, M.T., 1956. Cementation of Simpson and St. Peter sandstones in parts of Oklahoma, Arkansas, and Missouri. Journal of Geology 64, 16–30.

Helgeson, H.C., Knox, A.M., Owens, C.E., Shock, E.L., 1993. Petroleum, oil field waters, and authigenic mineral assemblages: are they in metastable equilibrium in hydrocarbon reservoirs? Geochimica et Cosmochimica Acta 57, 3295–3339.

Hering, J.G., Stumm, W., 1991. Oxidative and reductive dissolution of minerals. In: Hochella Jr., M.F., White, A.F. (Eds.), Mineral–Water Interface Geochemistry. Mineralogical Society of America, Reviews in Mineralogy 23, pp. 427–466.

Hickman, S.H., Evans, B., 1995. Kinetics of pressure solution at halite-silica interfaces and intergranular clay films. Journal of the Geological Society of London 148, 549–560.

Holeywell, R.C., Tullis, T.E., 1975. Mineral reorientation and slaty cleavage in the Martinsburg Formation, Lehigh Gap, Pennsylvania. Geological Society of America Bulletin 86, 1296–1304.

Housen, B.A., van der Pluijm, B.A., 1991. Slaty cleavage development and magnetic anisotropy fabrics. Journal of Geophysical Research 96, 9937–9946.

Housen, B.A., van der Pluijm, B.A., van der Voo, R., 1993a. Magnetite dissolution and neocrystallization during cleavage formation: Paleomagnetic study of the Martinsburg Formation, Lehigh Gap, Pennsylvania. Journal of Geophysical Research 98, 13,799–13,813.

Housen, B.A., Richter, C., van der Pluijm, B.A., 1993b. Composite magnetic anisotropy fabrics: experiments, numerical models, and implications for quantification of rock fabric. Tectonophysics 220, 1–12.

Hyeong, K., Capuano, R.M., 2001. Ca/Mg of brines in Miocene/Oligocene clastic sediments of the Texas Gulf Coast: buffering by calcite/disordered dolomite equilibria. Geochemica et Cosmochimica Acta 65, 3065–3080.

Imaz, A.G., Pocovi, A., Lago, M., Parés, J.M., 2000. Effect of lithostatic pressure and tectonic deformation on the magnetic fabric (anisotropy of magnetic susceptibility) in low-grade metamorphic rocks. Journal of Geophysical Research 105, 21,305–21,317.

Johnson, J.W., Oelkers, E.H., Helgeson, H.C., 1991. SUPCRT92: a software package for calculating the standard molal thermodynamic properties of minerals, gases, aqueous species, and reactions from 1 to 5000 bars and 0 to 1000 °C. Earth Sciences Department, Lawrence Livermore Laboratory.

Johnson, S.A., Turner, P., Hartley, A., Rey, D., 1995. Paleomagnetic implications for the timing of hematite precipitation and remagnetization in the Carboniferous Barren red Measures, UK southern North Sea. In: Turner, P., Turner, A. (Eds.), Paleomagnetic Applications in Hydrocarbon Exploration and production. Geological Society publication 98, pp. 97–117.

Juster, T.C., 1987. Mineralogic domains in very low grade politic rocks. Geology 15, 1010–1013.

Karato, S.-I., Masuda, T., 1989. Anisotropic grain growth in quartz aggregates under stress and its implications for foliation development. Geology 17, 695–698.

Karlin, R., 1990. Magnetic mineral diagenesis in suboxic sediments at Bettis site W–N, NE Pacific Ocean. Journal of Geophysical Research 95, 4421–4436.

Katz, B., Elmore, D., Cogoini, M., Engel, M., Ferry, S., 1998. Widespread chemical remagnetization: Orogenic fluids or burial diagenesis of clays? Geology 26, 603–606.

Katz, B., Elmore, D., Cogoini, M., Engel, M., Ferry, S., 2000. Associations between burial diagenesis of smectite, chemical remagnetization, and magnetite authigenesis in the Vocontian Trough, SE France. Journal of Geophysical Research 105, 851–868.

Kharaka, Y.K., Lico, M.S., Carothers, W.W., 1980. Predicted corrosion and scale-formation properties of geopressured-geothermal waters from the northern Gulf of Mexico basin. Journal of Petroleum Technology 32, 319–324.

Kharaka, Y.K., Law, L., Carothers, W.W., Goerlitz, D., 1986. Role of organic species dissolved in formation waters from sedimentary basins in mineral diagenesis. In: Gautier, D.L. (Ed.), Roles of organic matter in sediment diagenesis. Society of Economic Paleontologists and Mineralogists Special Publication 38, pp. 111–122.

Kodama, K.P., 1988. Remnance rotation due to rock strain during folding and stepwise application of the fold test. Journal of Geophysical Research 93, 3357–3371.

Kreutzberger, M.E., Peacor, D.R., 1988. Behavior of illite and chlorite during pressure solution of shaly limestone of the Kalkberg Formation, Catskill, New York. Journal of Structural Geology 10, 813–828.

Lagoeiro, L.E., 1998. Transformation of magnetite to hematite and its influence on the dissolution of iron oxide minerals. Journal of Metamorphic Geology 16, 415–423.

Leslie, B.W., Hammond, D.E., Berelson, W.M., Lund, S.P., 1990a. Diagenesis in anoxic sediments from the California borderland and its influence on iron, sulfur, and magnetite behavior. Journal of Geophysical Research 95, 4453–4470.

Leslie, B.W., Lund, S.P., Hammond, D.E., 1990b. Rock magnetic evidence for the dissolution and authigenic growth of magnetic minerals within anoxic marine sediments of the California continental borderland. Journal of Geophysical Research 95, 4437–4452.

Lewchuk, M.T., Evans, M.A., Elmore, R.D., 2002. Remagnetization signature of Paleozoic sediments from the Patterson Creek Anticline in West Virginia. Physics and Chemistry of the Earth 27, 1141–1150.

Lewchuk, M.T., Evans, M., Elmore, R.D., 2003. Synfolding remagnetization and deformation: results from the Paleozoic sedimentary rocks in West Virginia. Geophysical Journal International 151, 1–15.

Losh, S., Walter, L., Meulbroek, P., Martini, A., Cathles, L., Whelen, J., 2002. Reserrvoir fluids and their migration into the South Eugene Island Block 330 reservoirs, offshore Louisiana. American Association of Petroleum Geologists Bulletin 86, 1463–1488.

Lu, G., Marshak, S., Kent, D.V., 1990. Characteristics of magnetic carriers responsible for Late Paleozoic remagnetization in carbonate strata of the mid-continent, USA. Earth and Planetary Science Letters 99, 351–361.

Lu, G., McCabe, C., Hanor, J.S., Ferrell, R.E., 1991. A genetic link between remagnetization and potassic metasomatism in the Devonian Onondaga Formation, northern Appalachians. Geophysical Research Letters 18, 2047–2050.

Machel, H.G., 1995. Magnetic mineral assemblages and magnetic contrasts in diagentic environments—with implications for studies of paleomagnetism, hydrocarbon migration and exploration. In: Turner, P., Turner, A. (Eds.), Paleomagnetic Applications in Hydrocarbon Exploration and production. Geological Society Publication 98, pp. 9–29.

Machal, H.G., 2004. Bacterial and thermochemical sulfate reduction in diagenetic steeings—old and new insights. Sedimentary Geology 140, 143–175.

Majzlan, J., Grevel, K-D., Navrotsky, A., 2003. Enthalpies of formation and relative stability of goethite (α-FeOOH), lepidocrocite (γ-FeOOH) and maghemite (γ-Fe_2O_3). American Mineralogist 88, 855–859.

Markley, M., Wojtal, S., 1995. Mesoscopic structure, strain, and volume loss in folded cover strata, Valley and Ridge Province, Maryland. American Journal of Science 296, 23–57.

Marshak, S., Engelder, T., 1985. Development of cleavage in limestone of a fold-thrust belt in eastern New York. Journal of Structural Geology 7, 345–359.

McCabe, C., Van der Voo, R., Peacor, D.R., Scotese, C.R., Freeman, R., 1983. Diagenetic magnetite carries ancient yet secondary remanence in some Paleozoic sedimentary carbonates. Geology 11, 221–223.

McCaig, A.M., Knipe, R.J., 1990. Mass-transport mechanisms in deforming rocks: recognition using microstructural and microchemical criteria. Geology 18, 824–827.

McNeill, D.F., 1990. Biogenic magnetite from surface Holocene carbonate sediments, Great Bahama bank. Journal of Geophysical Research 95, 4363–4371.

Meike, A., Wenk, H.-R., 1988. A TEM study of microstructures associated with solution cleavage in limestone. Tectonophysics 154, 137–148.

Merino, E., Ortoleva, P., Strickholm, P., 1983. Generation of evenly-spaced pressure solution seams during late diagenesis: a kinetic theory. Contributions to Mineralogy and Petrology 82, 360–370.

Meyer, T.J., Dunne, W.M., 1990. Deformation of Helderberg limestones above the blind thrust system of the central Appalachians. Journal of Geology 98, 108–117.

Mimran, Y., 1977. Chalk deformation and large-scale migration of calcium carbonate. Sedimentology 24, 333–360.

Minissale, A., Vaselli, O., Chandrasekharem, D., Magro, G., Tassi, F., Casilia, A., 2000. Origin and evolution of 'intracratonic' thermal fluids from central-western peninsular India. Earth and Planetary Science Letters 181, 377–394.

Moldovanyi, E.P., Walter, L.M., 1992. Regional trends in water chemistry, Smackover Formation, southwest Arkansas: geochemical and physical controls. American Association of Petroleum Geologists Bulletin 76, 864–894.

Morad, S., Aldahan, A.A., 1982. Authignesis of titanium minerals in two Proterozoic sedimentary rocks from southern and central Sweden. Journal of Sedimentary Petrology 52, 1295–1305.

Morad, S., Aldahan, A.A., 1986. Alteration of detrital Fe–Ti oxides in sedimentary rocks. Geological Society of America Bulletin 97, 567–578.

Morton, R.A., Land, L.S., 1987. Regional variation in formation water chemistry, Frio Formation (Oligocene), Texas Gulf Coast. American Association of Petroleum Geologists Bulletin 71, 191–206.

Nesbitt, B., Muehlenbachs, K., 1995. Geochemical studies of the origins and effects of synorogenic crustal fluids in the southern Omineca Belt of British Columbia, Canada. Geological Society of America Bulletin 107, 1033–1050.

Parnell, J., 2004. Titanium mobilization by hydrocarbon fluids related to sill intrusion in a sedimentary sequence, Scotland. Ore Geology Reviews 24, 155–167.

Passchier, C.W., Trouw, R.A.J., 1996. Microtectonics. Springer, New York.

Posnjak, E., Merwin, H.E., 1922. The system, Fe_2O_3–SO_3–H_2O. Journal of the American Chemical Society 44, 1965–1994.

Raynaud, S., Carrio-Schaffhauser, E., 1992. Rock matrix structures in a zone influenced by a stylolite. Journal of Structural Geology 14, 973–980.

Reger, D.B., Tucker, R.C., 1924. Mineral and Grant Counties. West Virginia Geological Survey.

Rozanova, E.P., Borzenkov, I.A., Tarasov, A.L., Suntsova, L.A., Dong, Ch.L., Belyaev, S.S., Ivanov, M.V., 2001. Microbiological processes in a high-temperature oil field. Microbiology 70, 102–110.

Rutter, E.H., 1983. Pressure solution in nature, theory and experiment. Geological Society of London 140, 725–740.

Saffer, B., McCabe, C., 1992. Further studies of carbonate remagnetization in the northern Appalachian basin. Journal of Geophysical Research 97, 4331–4348.

Schmalz, R.F., 1959. A note on the system Fe_2O_3–H_2O. Journal of Geophysical Research 64, 575–579.

Schwander, H.W., Burgin, A., Stern, W.B., 1981. Some geochemical data on stylolites and their host rocks. Eclogae Geologicae Helveticae Acta 74, 217–224.

Shebl, M.A., Surdam, R.C., 1996. Redox reactions in hydrocarbon clastic reservoirs: experimental validation of this mechanism for porosity enhancement. Chemical Geology 132, 103–117.

Shipunov, S.V., 1997. Synfolding magnetizations: detection, testing, and geological applications. Geophysical Journal International 130, 405–410.

Shterev, K., Zagorchev, I., 1996. Mineral waters and hydrogeothermal resources in Bulgaria. GeoJournal 40, 397–403.

Smart, K.J., Dunne, W.M., Krieg, R.D., 1997. Roof response to emplacement of the Wills Mountain duplex: the roles of forethrusting and scales of deformation. Journal of Structural Geology 19, 1443–1459.

Smedley, P.L., Edmunds, W.M., 2002. Redox patterns and trace-element behavior in the East Midlands Triassic Sandstone aquifer, UK. Groundwater 40, 44–48.

Stamatakos, J., Hirt, A.M., Lowrie, W., 1996. The age and timing of folding in the central Appalachians from paleomagnetic results. Geological Society of America 108, 815–829.

Stoltz, J.F., Lovley, D.R., Haggerty, S.E., 1990. Biogenic magnetite and the mineralization of sediments. Journal of Geophysical Research 95, 4355–4361.

Suk, D., Peacor, D.R., Van der Voo, R., 1990a. Replacement of pyrite framboids by magnetite in limestone and implications for paleomagnetism. Nature 345, 611–613.

Suk, D., Van der Voo, R., Peacor, D.R., 1990b. Scanning and transmission electron microscope observations of magnetite and other iron phases in Ordovician carbonates from east Tennessee. Journal of Geophysical Research 95, 12,327–12,336.

Suk, D., Van der Voo, R., Peacor, D.R., 1991. SEM/STEM observations of magnetite in carbonates of eastern North America: evidence for chemical remagnetization during the Alleghanian orogeny. Geophysical Research Letters 18, 939–942.

Surdam, R.C., Crossey, L.J., 1985. Organic-inorganic reactions during progressive burial: key to porosity and permeability enhancement and preservation. Philosophical Transactions of the Royal Society of London A315, 135–156.

Surdham, R.C., Crossey, L.J., Hagen, E.S., Heasler, H.P., 1989. Organic-inorganic interactions and sandstone diagenesis. American Association of Petroleum Geologists Bulletin 73, 1–23.

Tada, R., Siever, R., 1989. Pressure solution during diagenesis. Annual Reviews of Earth and Planetary Science 17, 89–118.

Thomas, A.R., Dahl, W.M., Hall, C.M., York, D., 1993. $^{40}Ar/^{39}Ar$ analyses of authigenic muscovite, timing of stylolitization, and implications for pressure solution mechanisms: Jurassic Norphlet Formation, offshore Alabama. Clays and Clay Minerals 41, 269–279.

Tilton, J.L., Prouty, W.F., Tucker, R.C., Price, P.H., 1927. Hampshire and Hardy Counties. West Virginia Geological Survey.

Trurnit, P., 1968. Pressure solution phenomena in detrital rocks. Sedimentary Geology 2, 89–114.

Turner, P., Burley, S.D., Rey, D., Prosser, J., 1995. Burial History of the Penrith Sandstone (Lower Permian) deduced from the combined study of fluid inclusion and paleomagnetic data. In: Turner, P., Turner, A. (Eds.), Paleomagnetic Applications in Hydrocarbon Exploration and production. Geological Society Publication 98, pp. 43–78.

Varsanyi, I., Matray, J-M., Kovacs, L.O., 1999. Hydrogeochemistry in two adjacent areas in the Pannonian Basin (southeast-Hungary). Chemical Geology 156, 25–39.

Wanless, H.R., 1979. Limestone response to stress: pressure solution and dolomitization. Journal of Sedimentary Petrology 49, 437–462.

Waples, D.W., 1980. Time and temperature in petroleum formation: application of Lopatin's method to petroleum exploration. American Association of Petroleum Geologists Bulletin 64, 916–926.

Weaver, T.R., Frape, S.K., Cherry, J.A., 1995. Recent cross-formational fluid flow and mixing in the shallow Michigan Basin. Geological Society of America Bulletin 107, 697–707.

Weyl, P.K., 1959. Pressure solution and the force of crystallization—a phenomenological theory. Journal of Geophysical Research 64, 2001–2025.

Wilkins, R.T., Barnes, H.L., 1997. Formation processes of framboidal pyrite. Geochimica et Cosmochimica Acta 61, 323–339.

Wilson, T.H., Shumaker, R.C., 1992. Broadtop thrust sheet: an extensive blind thrust in the central Appalachians. American Association of Petroleum Geologists Bulletin 76, 1310–1324.

Wintsch, R.P., Kvale, C.M., Kisch, H.J., 1991. Open-system, constant-volume development of slaty cleavage, and strain-induced replacement reactions in the Martinsburg Formation, Lehigh Gap, Pennsylvania. Geological Society of America Bulletin 103, 916–927.

Xu, W., Van der Voo, R., Peacor, D.R., 1998. Electron microscopic and rock magnetic study of remagnetized Leadville carbonates, central Colorado. Tectonophysics 296, 333–362.